JOURNAL OF COMPUTATIONAL PHYSICS **130,** 25–40 (1997)
ARTICLE NO. CP965534

On Postshock Oscillations Due to Shock Capturing Schemes in Unsteady Flows

Mohit Arora* and Philip L. Roe

*Department of Aerospace Engineering, W. M. Keck Foundation Lab for Computational Fluid Dynamics, The University of Michigan, Ann Arbor, Michigan 48109-2118
E-mail: mohit@engin.umich.edu; philroe@engin.umich.edu

Received May 15, 1995; revised April 8, 1996

In this paper, the issue of postshock oscillations generated by shock-capturing schemes is investigated. Although these oscillations are frequently small enough to be ignored, there are contexts such as shock–noise interaction where they might prove very intrusive. Numerical experiments on simple nonlinear 2×2 systems of conservation laws are found to refute some earlier conjectures on their behavior. The trajectories in phase space of a computed state passing through a captured shock suggest the underlying mechanism that creates these oscillations. The results reveal a flaw in the way that the concept of monotonicity is extended from scalar conservation laws to systems; schemes satisfying this formal condition fail to prevent oscillations from being generated, even for monotone initial data. This indicates that satisfactory design criteria do not exist at the present time that would ensure captured shocks that are both narrow and free from oscillations.

1. INTRODUCTION

Over the last few decades, the technique of shock capturing has moved onto progressively firmer foundations. The original concept of von Neumann [23] was to add to the inviscid flow equations sufficient artificial viscosity to produce shock structures that could be resolved on the discrete grid. However, this almost amounted to a requirement that the shock should not be represented too narrowly. Then Lax and Wendroff [14] reinterpreted the schemes as solving the governing equations in integral rather than differential form, showing that in some average sense the correct jump relationships could be guaranteed as the mesh was refined if any stable, consistent scheme was expressed in "conservation form." This removed any need to represent pseudo-viscous structures with many mesh points. By making the internal structure appear irrelevant, the way was opened to modern techniques that resolve the shocks with very few "internal" values. Incidentally, Hou and Lax [11] give a nice interpretation of the von Neumann method and its relation to modern techniques.

Of course, at least one internal value is needed, so that a captured shock can be located anywhere on a one-dimensional grid (Fig. 1 (left)). A first-order finite-volume scheme with a flux function corresponding either to the exact solution of a Riemann problem [7] or else to Roe's [30] approximate solution does achieve this resolution for a steady one-dimensional shock. Recently, Jameson [12] and Liou [18] have called attention to economical classes of flux functions that share this property. The Osher flux function [25] gives rise to a family of shocks with two (exceptionally one) interior values (Fig. 1 (right)), as does the flux-vector splitting scheme of van Leer [36]. These properties are inherited by most modern high-order schemes using the same flux functions, because such schemes usually revert to their first-order counterparts sufficiently close to the shocks.[1]

This ability to classify methods and prove theorems about them contributes to a sense of understanding and controlling them, which may be somewhat illusory. It is well known that problems arise when the shock is not stationary but moves slowly across the mesh [38, 5, 29, 17, 28]. Small, but often noticeable, oscillations appear in those wave families not associated with the shock. Woodward and Colella [38] reported this phenomenon and suggested an explanation in terms of the quasi-steady shock structure. If we regard Fig. 1 (left) as snapshots of a moving shock then it is clear that the shock structure must actually be time dependent. It could perhaps be periodic in time, with period $T = h/S$, where h is the mesh size, S is the shock speed, and T is the time for the shock to move one mesh interval, after which its structure might be supposed to repeat. Clearly this argument is not exact, as T may not

* Current address: Morgan Stanley & Co. Inc., 750 Seventh Ave., 7th floor, New York, NY 10019.

[1] It is possible to prove [6] that a flux function $\mathbf{F}(u_L, u_R)$ which gives rise to one-point shocks cannot be a differentiable function of its input states. Since differentiability is a requirement for certain convergence techniques like Newton's method, the pursuit of maximal resolution may exact a toll. In practice, the question of convergence may be so complicated by other issues that this may not always be an important issue.

0021-9991/97 $25.00

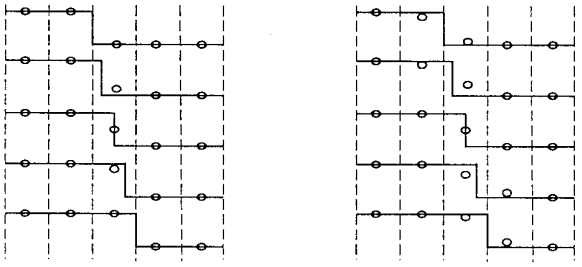

FIG. 1. In the figure on the left we show several cells (dashed lines) within which we have a shock (solid line). The numerical representation of this shock on this grid is represented by the cell centered values (o), for a scheme that has one internal state within the shock. We can regard this figure as snapshots of a shock moving to the right, captured at five different times, or as five different steady shocks. The figure on the right shows snapshots of the same shock captured by a two-point scheme.

be an integer, or even a rational, multiple of the timestep k, but numerical experiment makes it very plain that it contains substantial truth, because the spurious waves that are shed are very close to being periodic with period T, and hence have wavelength $\lambda h/S$, where λ is the speed of the wave carrying the oscillations.

A perfect shock-capturing scheme would not have such a flaw. Even though the oscillations might measure only a percentage or so of the shock jump that induces them (but we will demonstrate that this is not always so) that might be ruinous to delicate calculations of shock–sound interaction, for example. We would like to know if there are flux functions that do not suffer in this way, or if we are dealing with an unavoidable consequence of the shock-capturing strategy. If the latter, we would like to know a ranking order for the various schemes and flux functions.

If we could discover an underlying cause of the oscillations, we could perhaps design a scheme that was free of them. In fact, we believe that we have discovered a fundamental cause, but unfortunately it does not lead to a cure and leads us to suspect that no complete cure is possible without resorting to subcell resolution. The question would then become that of discovering a ranking order for the conventional schemes, although it seems to be the case that the actual ranking is rather problem-dependent.

Rigorous analysis is very difficult; it may be worth giving a brief history of what analysts have so far achieved. Jennings [13] studied travelling wave solutions for scalar conservation laws as computed by monotone difference schemes. He was able to prove that at large time the solution reached an asymptotic profile

$$u(j\,\Delta x, n\,\Delta t) = U(j\,\Delta x - Sn\,\Delta t),$$

where $U(\xi)$ is a continuous function and S is the speed of the analytical shock joining the left and right states. He found such a result for any strength of shockwave, provided the Courant number associated with shock speed, $\nu_S = S\,\Delta t/\Delta x$ was rational, $\nu_S = p/q$. Majda and Ralston [19] generalized this result to systems of equations solved by certain (not necessarily monotone) first-order schemes, provided the shocks were weak, but genuinely nonlinear. Michaelson [20] further extended the analysis to a certain third-order scheme and claimed in a footnote to be able to deal with schemes having any odd order of accuracy. For the Lax–Wendroff scheme, Smyrlis [34] found profiles for scalar problems with stationary shocks of any strength; Yu [40] has extended this to moving shocks and systems of equations provided the shocks are weak and ν_S is rational. Stationary structures for arbitrary shocks in systems, if computed by certain upwind schemes, have compact support and can be found relatively easily [25, 31, 36].

We believe that to shed any light on the problem discussed in this paper the analysis would need to deal with shocks that are not weak in systems of equations. The only permissible simplification would be to assume that S is small and to introduce a small parameter $\varepsilon = kS/h$, say, measuring the departure from a steady solution.

We have experimental evidence that such a scaling

$$u(x, t) = u_0(x - St) + \varepsilon u_1(x, t) + O(\varepsilon^2) \qquad (1.1)$$

would work, but that the function u_1 is extremely complicated. As a practical objective one might seek schemes for which the oscillations were small, perhaps with $u_1 = 0$. That would imply that moving shocks could be quasi-stationary (i.e., they would follow the same path in phase space as stationary shocks placed in varying locations). For most nonlinear systems this contradicts a second natural requirement, derived from simple conservation arguments in Section 5, and this is why we believe that no general cure is possible. Significantly, for special types of nonlinearity combined with special classes of data, there is no contradiction and no oscillations occur.

The fact that a quasi-steady analysis is feasible in principle makes it clear that steady structure is relevant to unsteady structure, although it leaves the nature of the influence uncertain. Intuitively, one might speculate that two-point structures (Fig. 1 (right)) yield less noise than one-point structures, because they are somehow smoother. For the Euler equations, this speculation was apparently confirmed by the numerical experiments of Roberts [29], who found in addition that, among the class of 2-point schemes, the O-version of Osher's method produced lower amplitude oscillations than the (less expensive) P-version. Our revisiting of this problem was partly motivated by experiments revealing that the order of merit is reversed when the schemes are applied to a simple p-system. This, and other experiments on simple first-order schemes are reported in Section 2.

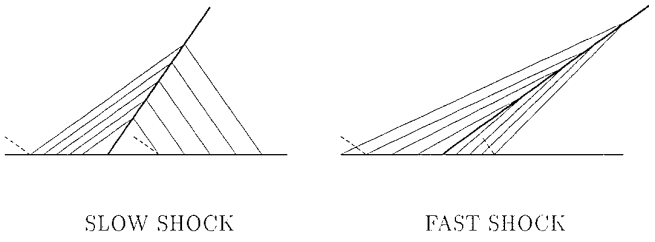

FIG. 2. Definition of slow and fast shocks. The characteristic belonging to the shock family changes sign across a slow shock. The small dashed lines represent the characteristic of the other family.

Another piece of folk-lore is that the spurious oscillations only affect slowly moving shocks (where slowly moving is sometime interpreted as meaning that the wavespeed associated with the shock changes sign across it (Fig. 2). Our more detailed studies show that the difference between these and other shocks is only a matter of degree. Indeed, the folklore is refuted by the occurrence of oscillations in the *p*-system, which admits only fast shocks (as does any Lagrangian system).

The concept of monotonicity is introduced in Section 3, followed by its commonly used extension to nonlinear systems. We question, however, whether schemes satisfying this extension are ''monotone'' or ''total variation diminishing'' in any practically meaningful sense.

Roberts displayed his results by tracking, in conserved-variable phase space, the trajectory of a given mesh point as the shock traverses it. We experimented with superposing the tracks of all mesh points. This has the advantage of allowing the trajectories of fast-moving shocks to be seen. Even though each grid point would contribute only a few points to the trajectory as the shock sweeps by it, the ensemble of points paint a much more detailed picture, reminiscent of the strange attractors occurring in dynamical systems. We present several of these phase portraits in Section 4, in the belief that, not only are they entertaining and picturesque, but they also display clearly the complexity of the problem. Usually we present our portraits in the space of characteristic variables.

In Section 4, we also consider second-order schemes. Not surprisingly, the Lax–Wendroff scheme generates large oscillations, as it would do even for a linear problem, but a flux-limited version of Lax–Wendroff yields a phase portrait very similar to (even though not identical with) the first-order scheme using the same Riemann solver. This seems to confirm that if we could devise a good first-order scheme, it would extend easily to second order.

Unfortunately, our findings in Section 5 suggest that a good first-order scheme may not be, in general, achievable. All of the trajectories we present seem to show the competing effects of two equally desirable ideal trajectories. One of these is the quasi-steady trajectory; the other is simply a straight line in the space of conserved variables. Actual trajectories give the impression of attempting to compromise between these. We confirm the hypothesis by constructing a quadratic flux function and a class of data for which the two trajectories coincide. There is then no conflict and no oscillation. For ''real'' equation sets and data, the conflict appears unavoidable.

In Section 6 we speculate on strategies that might be used to alleviate the problem in practice. None of them is simple, and we have not seriously attempted to implement any of them.

2. DIFFICULTIES WITH MOVING SHOCKS

2.1. Some First-Order Schemes Applied to Simple Conservation Laws

The general form of the conservation laws we consider is

$$\mathbf{w}_t + \mathbf{f}_x = 0, \quad \mathbf{w}(t=0) = \mathbf{w}_0, \tag{2.1}$$

where $\mathbf{w}, \mathbf{f}$ are the vectors of state and flux variables, respectively. The conservative discretization of Eq. (2.1) is

$$\mathbf{w}^j = \mathbf{w}_j - \tau(\mathbf{F}_{j+1/2} - \mathbf{F}_{j-1/2}), \tag{2.2}$$

where $\mathbf{w}^j$ is the state vector at the new time level in cell j while $\mathbf{w}_j$ is that at the old time level. The quantity $\mathbf{F}_{j+1/2}$ is the numerical flux function at the interface between cells $(j, j+1)$, and $\tau = \Delta t/\Delta x$ is the mesh ratio. We create first-order schemes by defining $\mathbf{F}_{j+1/2}$ to be the solution (by some exact or approximate method) of the Riemann problem with data $\mathbf{w}_j, \mathbf{w}_{j+1}$.

For each system of conservation laws, we will choose initial conditions corresponding to Riemann data

$$\mathbf{w}_0 = \begin{cases} \mathbf{w}_\mathrm{L}, & x < 0 \\ \mathbf{w}_\mathrm{R}, & x > 0. \end{cases}$$

Further, we will choose $\mathbf{w}_0$ such that the solution to the Riemann problem is a single front-shock.

For each conservation law that we solve, we select in this section a first-order numerical flux function and compare the relative merits of the numerical schemes. This enables us to determine whether this phenomenon is dependent on the particular system being solved and whether a particular numerical flux function is to be preferred.

2.2. The p-System

One of the simplest examples of a 2×2 system is the *p*-system [33], which is Eq. (2.1) with

$$\mathbf{w} = (v, u)^\mathrm{T}, \quad \mathbf{f} = (-u, p)^\mathrm{T}, \quad p = p(v), \tag{2.3}$$

with $p_v(v) < 0$, $p_{vv}(v) > 0$. Here we take $p = v^{-2}$. These equations form a system of hyperbolic conservation laws in Lagrangian coordinates, with eigenvalues given by

$$\lambda_{1,2} = \mp [-p_v(v)]^{1/2}.$$

The characteristic equations are

$$du - \lambda_{1,2} \cdot dv = 0, \quad \text{along } \frac{dx}{dt} = \lambda_{1,2},$$

which are easily integrated to give the characteristic variables explicitly as

$$C^{\mp} = u \mp \left(\frac{8}{v}\right)^{1/2}. \tag{2.4}$$

These variables serve as a natural coordinate frame in which to visualize this phenomenon and to assist our investigation into the underlying mechanism generating these oscillations. The shock and rarefaction curves can be easily derived and are given in [33]. Because the wavespeeds are always of opposite sign, shocks in the p-system are always fast as defined above.

2.2.1. *Observations for the p-System*

Equation (2.2) was solved numerically with the Roe [30] and Osher [25] schemes, and the results for the back-characteristic variable C^- are shown in Fig. 3, from which we see that this variable (C^-) has a persistent postshock error. This wavelength (l_{error}) of the error is given approximately by [29]

$$l_{\text{error}} = \frac{\lambda_L^{(1)}}{S}\Delta x = \frac{[-p_v(v_L)]^{1/2}}{S}\Delta x.$$

We will demonstrate in Section 4 that the characteristic variable belonging to the shock family (i.e., the front-characteristic C^+) is not monotone either. Thus, the problem is not restricted to slow shocks and does not manifest itself only in the "other" characteristic variable.

Roberts [29] found a definite ordering among the schemes that he tested. For a first-order scheme, he observed that the exact Riemann solution and Roe's approximate Riemann solver gave the largest oscillations, followed by the P version of Osher's solver (where the left and right states are connected by simple waves ordered from the smallest to the largest eigenvalue, which is intuitively more physical). Best was the O version of Osher's solver (here, the eigenvalues are ordered from the largest to the smallest—this is the true Osher path).

For our experiments with the p-system, this ordering was exactly reversed (Fig. 3). Also, the errors are not small—they are of the same order as the actual jump at the shock. Thus, several features of shock oscillations previously conjectured to be universal turn out to be peculiar to the equation set concerned.

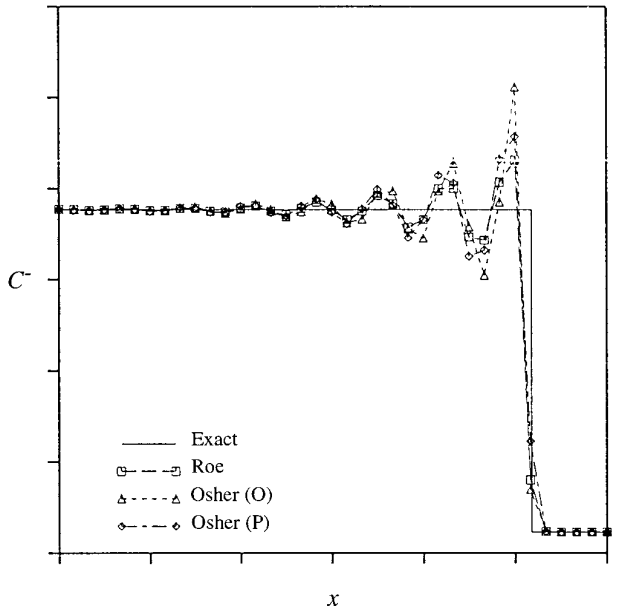

FIG. 3. A typical result for the p-system, with data $\mathbf{w}_L = (1, 1)^T$, $\mathbf{w}_R = (50.981, -6.068)^T$, solved for the Roe scheme and the Osher schemes (both the O and P variants). We plot here the 1-characteristic variable (C^-) as a function of position for these first-order schemes superposed onto the exact solution. This data results in a 2-shock, which is fast, because the eigenvalues for this system do not change sign across the shock. Note that the errors are a large percentage of the actual jump at the shock. The vertical view window is $\Delta C^- = 0.75$.

2.3. The Isothermal Euler Equations

For this system, the vectors in Eq. (2.1) are

$$\mathbf{w} = (\rho, \rho u)^T, \quad \mathbf{f} = (\rho u, \rho u^2 + \rho a^2)^T, \quad a = \text{const}, \tag{2.5}$$

with wavespeeds

$$\lambda_{1,2} = u \mp a. \tag{2.6}$$

The characteristic equations and characteristic variables are

$$d\left(\ln \rho \mp \frac{u}{a}\right) = 0, \quad \text{along } \frac{dx}{dt} = u \mp a,$$
$$C^{\mp} = \ln \rho \mp \frac{u}{a}. \tag{2.7}$$

The shock and rarefaction curves are derived in [15].

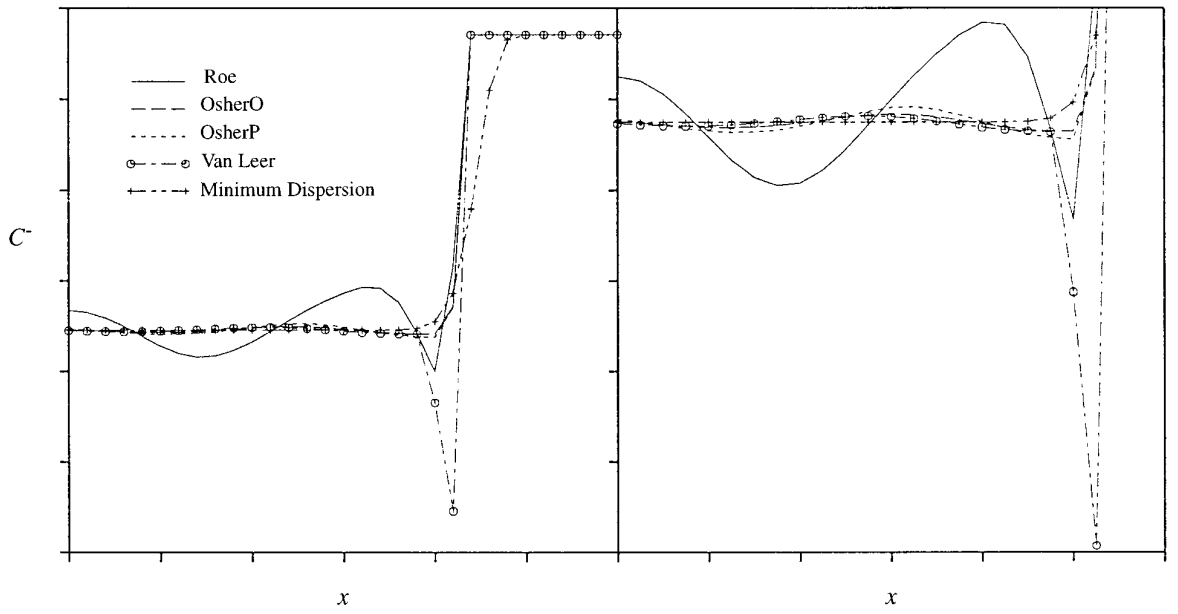

FIG. 4. Here, we have plotted the 1-characteristic variable (C^-) as a function of position for the isothermal Euler equations for stationary shock data $\mathbf{w}_L = (4, -2)^T$, $\mathbf{w}_R = (1, -2)^T$, with a superposed convective velocity $u_c = 0.1 = S$. We present a comparison of results obtained by the Roe scheme, the Osher schemes (O and P), Van Leer's FVS scheme, and the minimum dispersion scheme. The figure on the right is a zoom of the postshock values for the various schemes, showing their oscillatory behavior. The vertical view window is $\Delta C^- = 0.21$ for the figure on the left and $\Delta C^- = 0.09$ for the zoom on the right.

2.3.1. *Observations for the Isothermal Euler Equations*

Numerical results for the Roe [30] and Osher [24]) schemes as well as Van Leer's FVS [36] scheme are presented in Fig. 4. These results are consistent with those of Roberts [29], in that we see the ordering of schemes as he did, i.e., the true Osher, reversed Osher and Roe, in order of increasing amplitude of errors. Note further, that for the FVS scheme, we have a large error in the numerical shock layer, while the errors are comparable to the Osher schemes elsewhere. We shall return to the nonmonotonicity of the FVS scheme and its implications later (Section 6).

In addition, we tested one scheme not linearly equivalent to first-order upwinding. We speculated that disturbances of the same family as the shock might be escaping from it due to phase error, so that some improvement might result from using a scheme linearly equivalent to the minimum dispersion scheme [4] (note that in our implementation, we have used the Roe matrix in place of the exact Jacobian matrix). This was a partial success, in that this scheme, based on Roe's Riemann solver, produced results that had oscillations in the C^- variable of less than one part in 10,000 (for the cases we computed); however, the shock profiles were considerably broadened (see Fig. 4).

2.4. The Full Euler Equations

The state and flux vectors of Eq. (2.1) are

$$\mathbf{w} = (\rho, \rho u, \rho E)^T, \quad \mathbf{f} = (\rho u, \rho u^2 + p, \rho u H)^T, \tag{2.8}$$

where the equation of state required for closure is $p(\rho, e) = (\gamma - 1)\rho e$, $\gamma = c_p/c_v = 1.4$ is the ratio of specific heats, and e is the specific internal energy. In the above equation, the specific total energy is $E = e + u^2/2$ and the specific total enthalpy is $H = E + p/\rho$. This system has eigenvalues

$$\lambda_{1,2,3} = u - a, u, u + a, \tag{2.9}$$

and characteristic equations

$$dp \mp \rho a du = 0, \quad \text{along } \frac{dx}{dt} = \lambda_{1,3},$$

$$dp - a^2\, d\rho = 0, \quad \text{along } \frac{dx}{dt} = \lambda_2.$$

See [8] for the shock and rarefaction curves.

2.4.1. *Observations for the Full Euler Equations*

Numerical results for the Roe scheme are presented in Fig. 5, and we were able to duplicate the observations of Roberts [29] for this case as well; however, we found that several shock-tube problems, which appeared to be free of this phenomenon, were only so to plotting accuracy—zooming in revealed the now-familiar oscillations (Fig. 6).

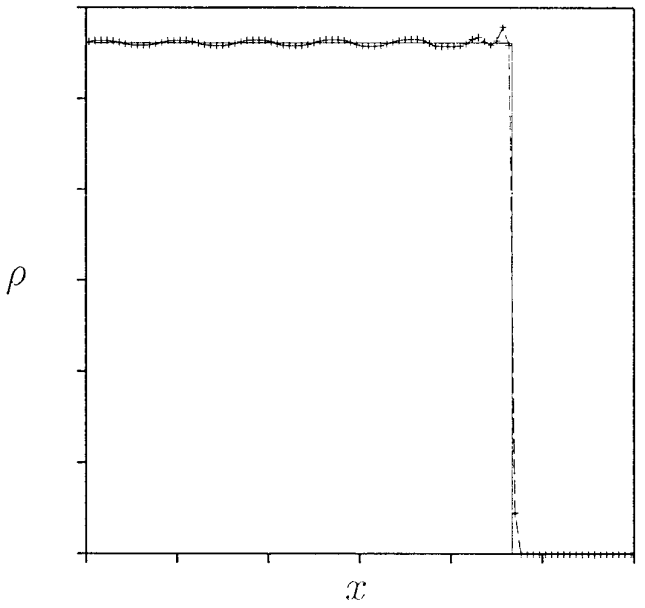

FIG. 5. A typical plot of the density for the solution to the Euler equations with primitive variable data ($\mathbf{w} = (\rho, u, p)^{\mathrm{T}}$) $\mathbf{w}_{\mathrm{L}} = (0.3061, -0.6821, 0.5908)^{\mathrm{T}}$, $\mathbf{w}_{\mathrm{R}} = (0.1, -2.5, 0.1)^{\mathrm{T}}$, using a second-order flux-limited Lax–Wendroff scheme with the Roe scheme as the underlying first-order scheme. This gives a shock speed $S = 0.2$, and we used a CFL number of 0.81 and Van Leer's harmonic limiter. The solid line is the exact solution while the dashed line with symbols is the numerical solution. The vertical view window is $\Delta\rho = 0.22$.

3. A DIGRESSION ON MONOTONICITY

When solving a scalar problem by a method of the form

$$u^j = u^j(u_{j-k}, ..., u_{j+k})$$

the scheme is said to be monotone [13] if

$$\frac{\partial u^j}{\partial u_m} \geq 0, \quad \forall\, m = j-k, ..., j+k. \tag{3.1}$$

Harten [9] established this concept as the most restrictive member of a hierarchy of design constraints for numerical schemes, which can be concisely written as

$$\text{Monotone} \Rightarrow L_1 - \text{contracting},$$

$$L_1 - \text{contracting} \Rightarrow \text{Total variation diminishing},$$

$$\text{Total variation diminishing} \Rightarrow \text{Monotonicity preserving}.$$

For monotone schemes Jennings [13] proved the existence of travelling wave solutions, which are the orbits for the scalar conservation laws that he studied. By this we mean that all u_j^n, for $(n - j)$ large enough, are close to a continuous function $u(\xi)$, where

$$\xi = j - n\nu_S, \tag{3.2}$$

and $\nu_S = S\,\Delta t/\Delta x$ is the CFL number based on the shock speed S. This establishes that given a conservation law, a numerical scheme meeting certain conditions and some initial data, this orbit is fully determined. Properties of the orbits were established in greater detail by Majda and Ralston [19].

This monotonicity concept has been extended to systems of conservation laws as a guiding principle in the design of numerical algorithms. The extended principle is precisely the basis for the splitting of fluxes in FVS schemes, demanding the eigenvalues of split fluxes be nonnegative for $\mathbf{F}^+$ and nonpositive for $\mathbf{F}^-$ (i.e., $\lambda^+ \geq 0$, $\lambda^- \leq 0$). However, from the FVS results for the isothermal Euler equa-

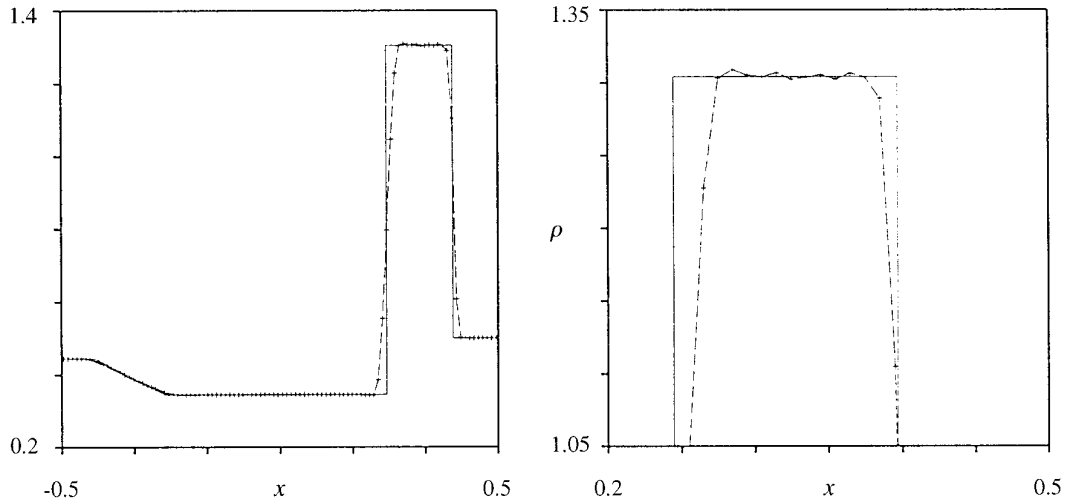

FIG. 6. Solution to the Lax problem for the Euler equations, with primitive variable data ($\mathbf{w} = (\rho, u, p)^{\mathrm{T}}$ $\mathbf{w}_{\mathrm{L}} = (0.445, 0.698, 3.528)^{\mathrm{T}}$, $\mathbf{w}_{\mathrm{R}} = (0.5, 0.0, 0.571)^{\mathrm{T}}$, using a second-order flux-limited Lax–Wendroff scheme with the Roe scheme as the underlying first-order scheme. These results show that although the region behind the shock (and in front of the contact), looks oscillation-free (left), these are present as seen in the zoom (right).

tions shown in Section 2.3.1 (Fig. 5), we clearly see that, although by construction the scheme is technically monotone, this has not succeeded in enforcing any of the qualitative properties we might have hoped for.

Thus, even the most restrictive of Harten's hierarchy of constraints does not translate in any convincing way to nonlinear systems. In fact, it seems that for systems, "monotone" does not imply "monotonicity preserving."

4. VISUALIZATION IN STATE SPACE—ORBIT PLOTS

In the course of analyzing the data for the 2×2 systems (Section 2), we have found that an efficient method of representing all the relevant information in a single picture is to make iterative maps in phase space, using characteristic variables (C^-, C^+) as coordinates. The results provide much insight into the process of postshock oscillations and reveal some interesting behavior. Based on our experiments, we make the following claim.

Let P_j^n be points in phase space generated in the one-dimensional numerical simulation of a moving nonlinear discontinuity, for some given set of conservation laws, using any stable deterministic algorithm, on a fixed mesh with spacings $(\Delta x, \Delta t)$. Here, n is the time level and j is the cell number. Then, as n increases, all such points approach indefinitely close to a limiting curve which can be parameterized by the variable ξ (Eq. (3.2)). Our experiments seem to show that such orbits exist for any stable deterministic algorithm (for example, second-order methods such as the Lax–Wendroff and Beam–Warming schemes, as well as algorithms constructed using nonlinear limiters) and for any nonlinear system we have explored, provided the discontinuity belongs to a genuinely nonlinear family.

The orbits must of course connect the two points in phase space that represent the pre- and postshock states. Typically, the orbit leaves one of these endpoints smoothly, and spirals into the other, following something like a damped version of a Lissajous figure (a curve generated in the plane by a particle simultaneously moving sinusoidally in two mutually perpendicular directions). However, a spiral at each end is possible (some examples of these will be shown shortly). We suppose that these parts of the orbit could be explained by linearizing the equations around one of the asymptotic states. The intermediate part of the orbit can, however, display considerable individuality depending on the governing equations and the scheme employed. It is certainly remarkable that each excursion is faithfully reproduced at all later stages in the history of the evolving discontinuity. This is most readily observed by color-coding the history of the points in time (Figs. 7 and 8), from which we can see how transient points are "pulled" towards this limiting (attracting) orbit (Fig. 9), after which all subsequent points lie on this limit curve (Figs. 8 and 9). The color-code used in the orbit plots is a transition from blue ($t = 0$) to red ($t = T$, the final time), with the intermediate times corresponding to intermediate colors (blue to green to yellow to red, in order of increasing time). Note that in the phase portraits, we have plotted $P_j^n \ \forall j, n$, on the same picture. The simultaneous oscillations in the (mutually perpendicular) C^-, C^+ directions gives rise to Lissajous figures, which directly represent the trailing oscillatory wavetrain.

In addition, observe from Figs. 7 and 9 that the final orbit loops over the state L, indicating that there is an overshoot in the C^+ variable (the y-coordinate in the orbit plots); this point was made in Section 2, but not demonstrated there.

In Fig. 10, we plot orbits for the first-order Roe scheme to see the effect of small nonzero S (for the isothermal Euler equations). In the limit of $S \to 0$, we expect our orbit to be the Hugoniot because for a stationary shock the Roe solver gives us a single intermediate state lying on the Hugoniot [31]. Thus, the Hugoniot curve H is a limiting case of a shock orbit, interpreted as the set of all intermediate states obtainable from arbitrary initial conditions (but with L, R connected by a single shock). Figure 10 is empirical evidence that for $S = \varepsilon$, the orbit departs from H by $O(\varepsilon)$.

In Fig. 11, we present orbits for the minimum dispersion scheme and Van Leer's FVS scheme, while in Fig. 12, we plot these for Osher's O and P variants. Observe that the orbit for the minimum dispersion scheme approaches the Hugoniot, appearing to be tangential near the postshock state (to the naked eye). The O version of Osher's scheme is close to the Hugoniot, but oscillatory behaviour is visible, becoming more pronounced for Osher's P version. Van Leer's FVS scheme and Roe's scheme are quite oscillatory near the postshock state for this system, giving the impression that they are constantly overcompensating for the error.

Figure 13 shows second-order schemes using the minmod and Van Leer's (harmonic) limiters (here, we use flux limiting, with a wave-by-wave limiting procedure for each equation [2]—for more details on limiting, see [35]). These can be compared to Fig. 10 (left) to see that the orbits for the limited second-order schemes are very similar to that of the basic first-order scheme. It is seen that as the schemes get better, the second crossover of the orbit with the Hugoniot (near L) moves closer to L, while the first crossover point stays almost stationary. The fact that the second-order flux-limited schemes shown in Fig. 13 closely resemble the underlying Roe scheme comes as no surprise, since in the vicinity of shocks, we expect the scheme to reduce to the underlying first-order scheme.

The pure Lax–Wendroff scheme (with no limiting) provides some very interesting orbits. First, we get Lissajous figures at each end of the Hugoniot (Fig. 14). Second, if we zoom in on the lower lobe, we find a qualitatively

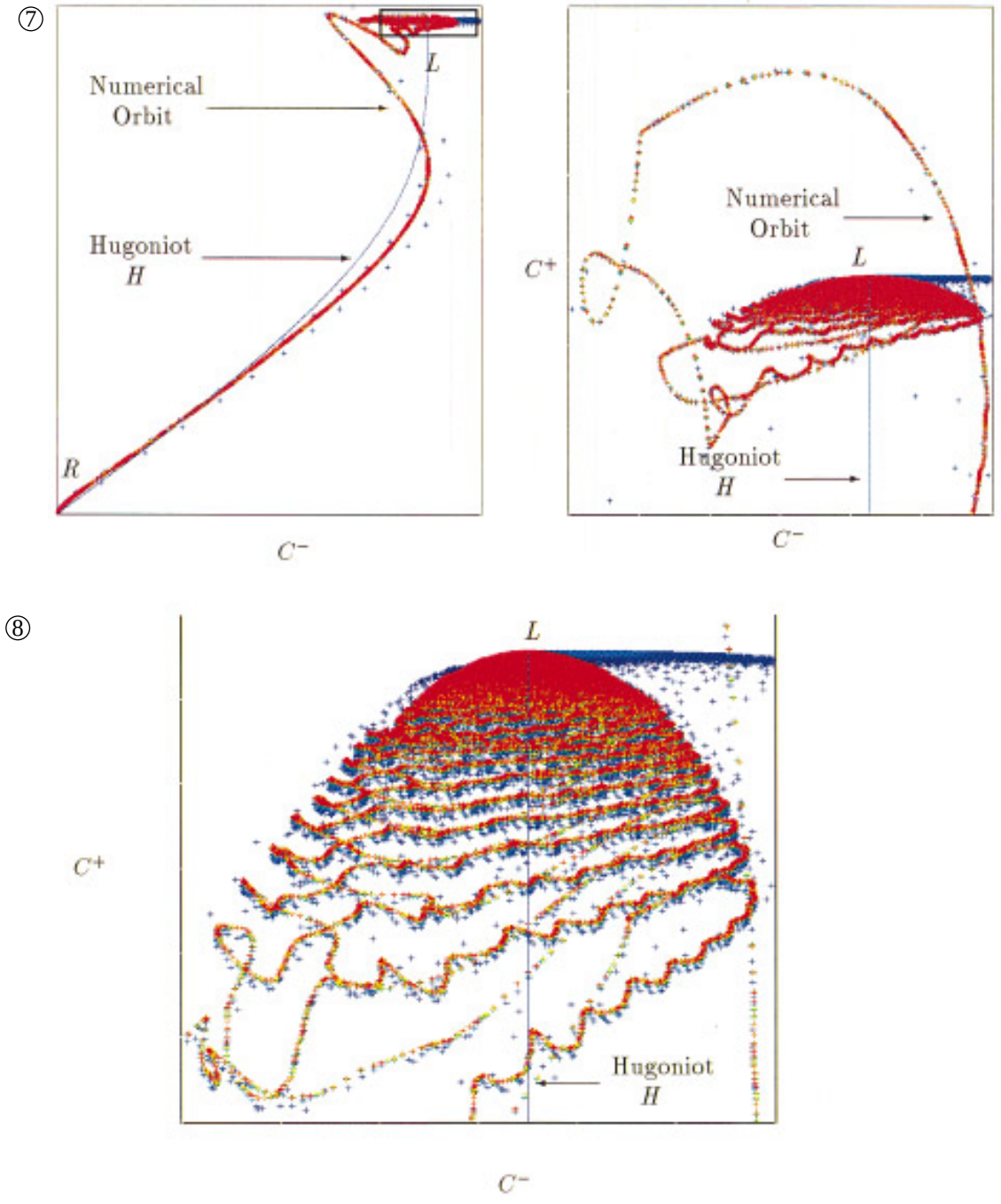

FIG. 7. Orbit plots for the *p*-system using the first-order Roe scheme with $\mathbf{w}_L = (1, 1)^T$, $\mathbf{w}_R = (50.981, -6.068)^T$. The figure on the left shows the Hugoniot and the numerical orbit (the stray points are simply the early time transients). On the right is a zoom of the boxed area (schematic), showing that the ''other'' characteristic variable is non-monotone (since it is seen to loop over the value at the left state (L). We also get a first glimpse at the intricacies of the orbit. The view window for the plot on the left is approximately $\Delta C^- = 5.31$, $\Delta C^+ = 9.8$, while that for the plot on the right is approximately $\Delta C^- = 1.25$, $\Delta C^+ = 0.162$.

FIG. 8. A further zoom of the region shown in Fig. 7 (right) showing the details of the orbit. It is quite extraordinary that the orbit loops over itself among other things and that all points lie on such an orbit. The view window for this plot is approximately $\Delta C^- = 0.85$, $\Delta C^+ = 0.0263$.

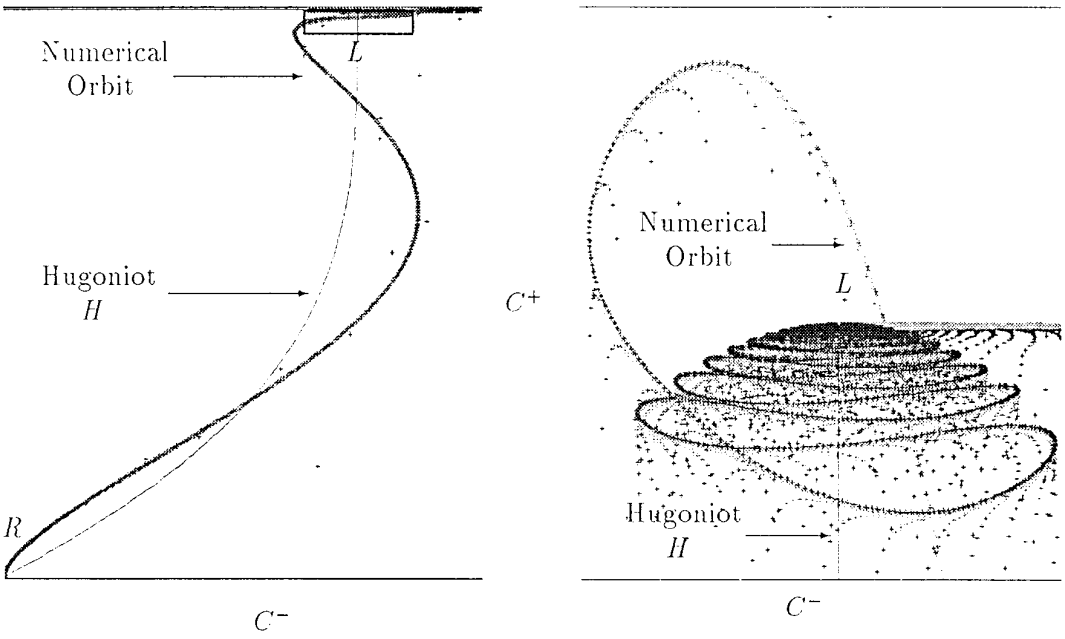

FIG. 9. Orbit plots (similar to Fig. 7) for the *p*-system using the first-order Roe scheme with $w_L = (1, 1)^T$, $\mathbf{w}_R = (5.342, -1.047)^T$, which is a weaker (faster) shock. This results in orbit that are more smooth, but qualitatively, the behavior is similar to the previous case. Once again, the "other" characteristic variable is nonmonotone and the orbit is intricate. Another feature, more clearly seen here, is the manner in which the points are *attracted* to the orbit. The view window for the plot on the left is approximately $\Delta C^- = 0.61$, $\Delta C^+ = 3.7$, while that for the plot on the right is approximately $\Delta C^- = 0.122$, $\Delta C^+ = 0.00286$.

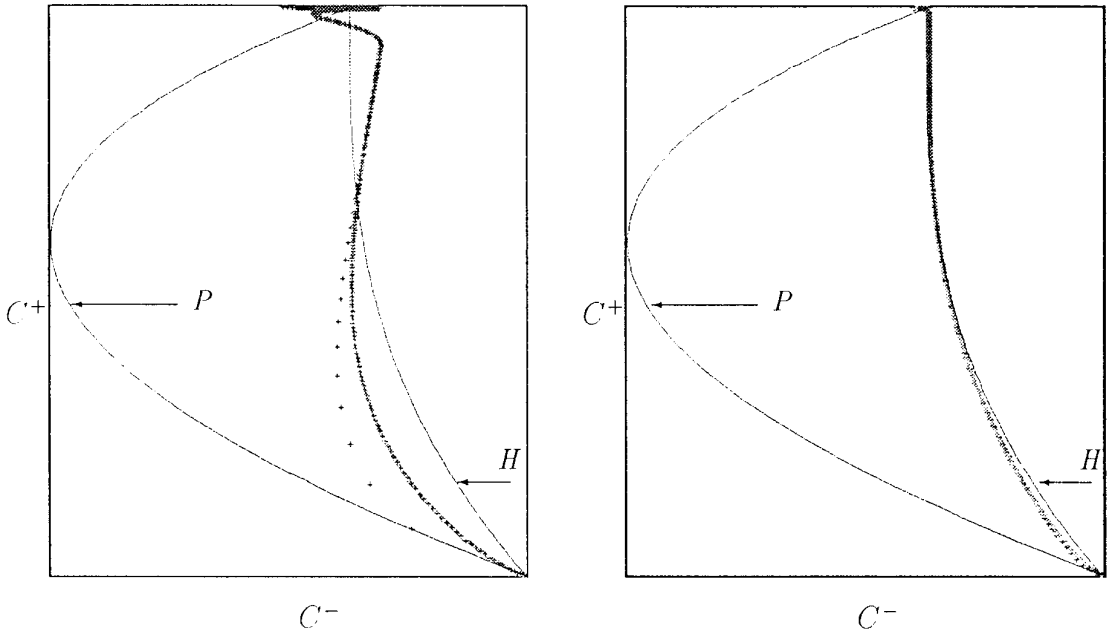

FIG. 10. Orbit plots for the isothermal Euler equations using the first-order Roe scheme with stationary shock data $\mathbf{w}_L = (4, -2)^T$, $\mathbf{w}_R = (1, -2)^T$, with a superposed convective velocity $u_c = S = 0.1$ (left), 0.01 (right). As can be seen, the behavior of the scheme is essentially the same, and as $S \to 0$, the limiting curve approaches the Hugoniot. Also shown is the projection (P), which is the path a moving discontinuity actually follows (it is the straight line joining the left and right states in conserved variable space, projected here onto characteristic variable space). The view window for these plots is approximately $\Delta C^- = 0.31$, $\Delta C^+ = 2.9$.

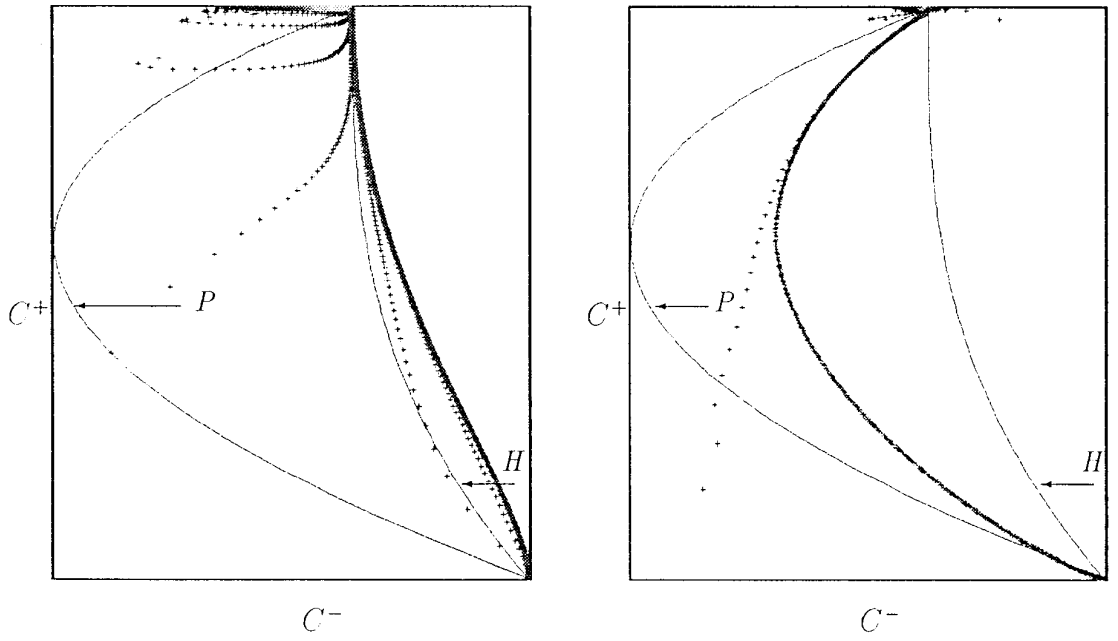

FIG. 11. Orbit plots for the isothermal Euler equations using the minimum dispersion scheme (left) and Van Leer's flux vector splitting (FVS) scheme (right), with stationary shock data $\mathbf{w}_L = (4, -2)^T$, $\mathbf{w}_R = (1, -2)^T$, with a superposed convective velocity $u_c = 0.1 = S$. The view window for these plots is approximately $\Delta C^- = 0.31$, $\Delta C^+ = 2.9$.

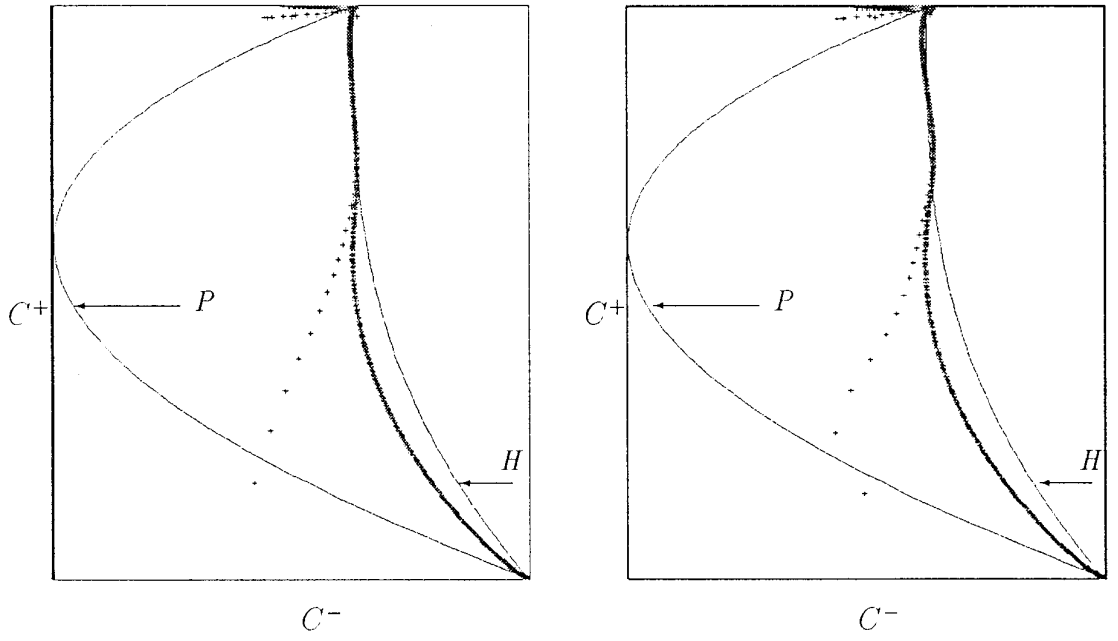

FIG. 12. Orbit plots for the isothermal Euler equations using the first-order Osher schemes with stationary shock data $\mathbf{w}_L = (4, -2)^T$, $\mathbf{w}_R = (1, -2)^T$, with a superposed convective velocity $u_c = S = 0.1$ for the O (left) and P (right) variants. The view window for these plots is approximately $\Delta C^- = 0.31$, $\Delta C^+ = 2.9$.

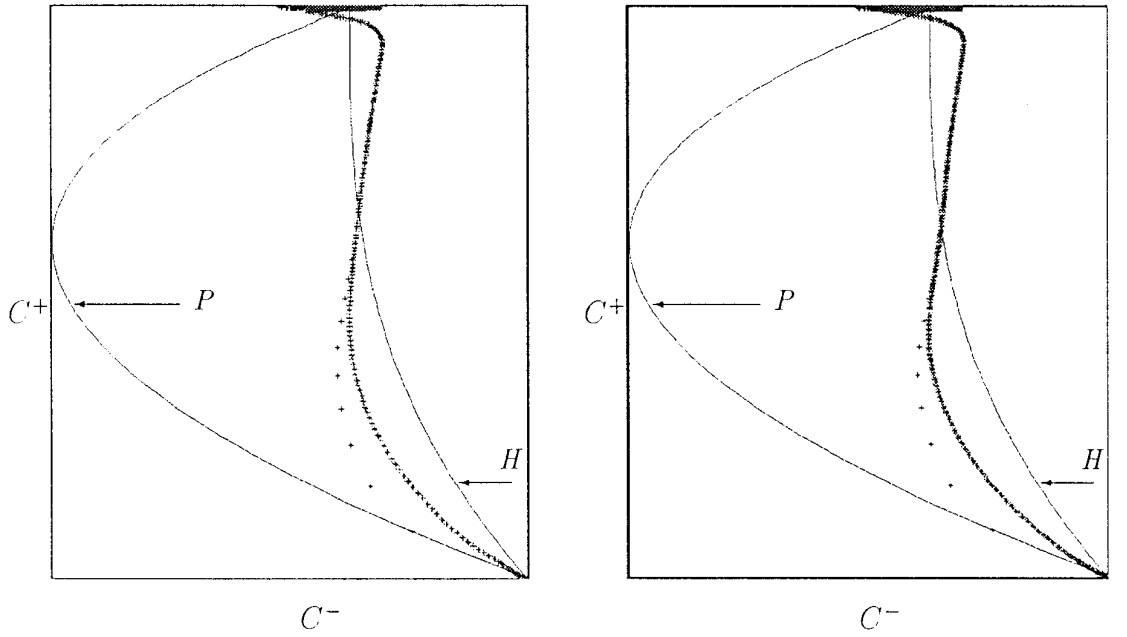

FIG. 13. Orbit plots for the isothermal Euler equations using a flux-limited, explicit, Roe-averaged Lax–Wendroff scheme with stationary shock data $\mathbf{w}_L = (4, -2)^T$, $\mathbf{w}_R = (1, -2)^T$, with a superposed convective velocity $u_c = 0.1 = S$. The figure on the left (right) was obtained using the minmod (Van Leer's harmonic) limiter. The view window for these plots is approximately $\Delta C^- = 0.31$, $\Delta C^+ = 2.9$.

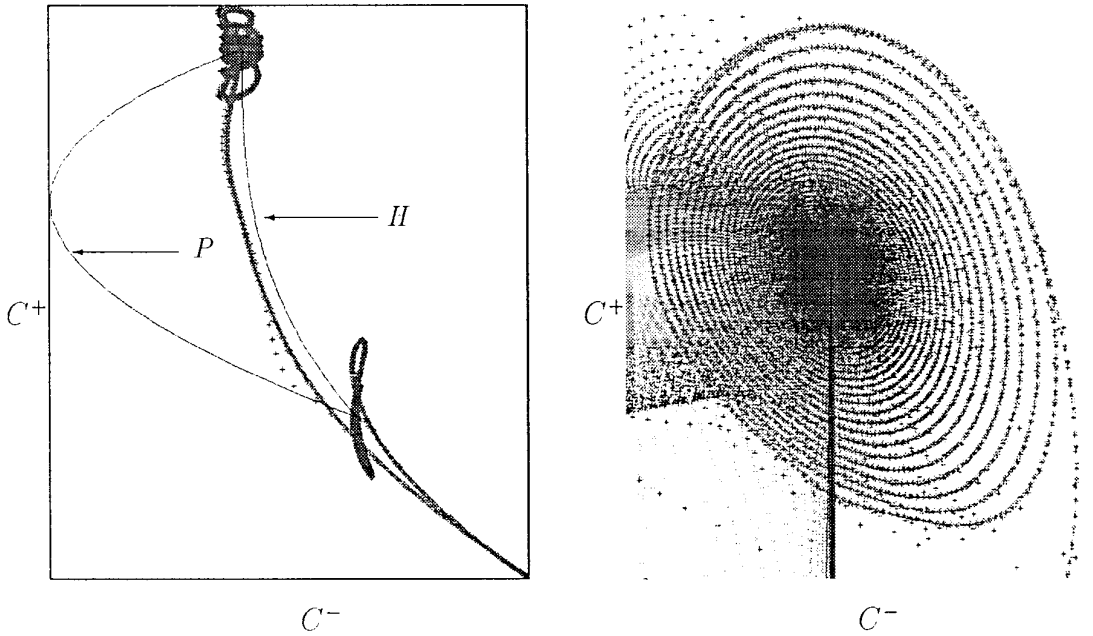

FIG. 14. This plot is to demonstrate that Lissajous figures and spirals form, and sometimes are remarkably clear. These are orbit plots for the isothermal Euler equations using the unlimited second-order Lax–Wendroff scheme (left) and a zoom of Van Leer's FVS scheme (shown in Fig. 11 (right)), with stationary shock data $\mathbf{w}_L = (4, -2)^T$, $\mathbf{w}_R = (1, -2)^T$, with a superposed convective velocity $u_c = S = 0.1$. The Lax–Wendroff scheme gives very nice Lissajous figures at both ends, and the Van Leer scheme shows the states spiralling into the left state. The view window for the plot on the left is approximately $\Delta C^- = 0.5$, $\Delta C^+ = 4.55$, while that for the plot on the right is approximately $\Delta C^- = 0.0035$, $\Delta C^+ = 0.0005$.

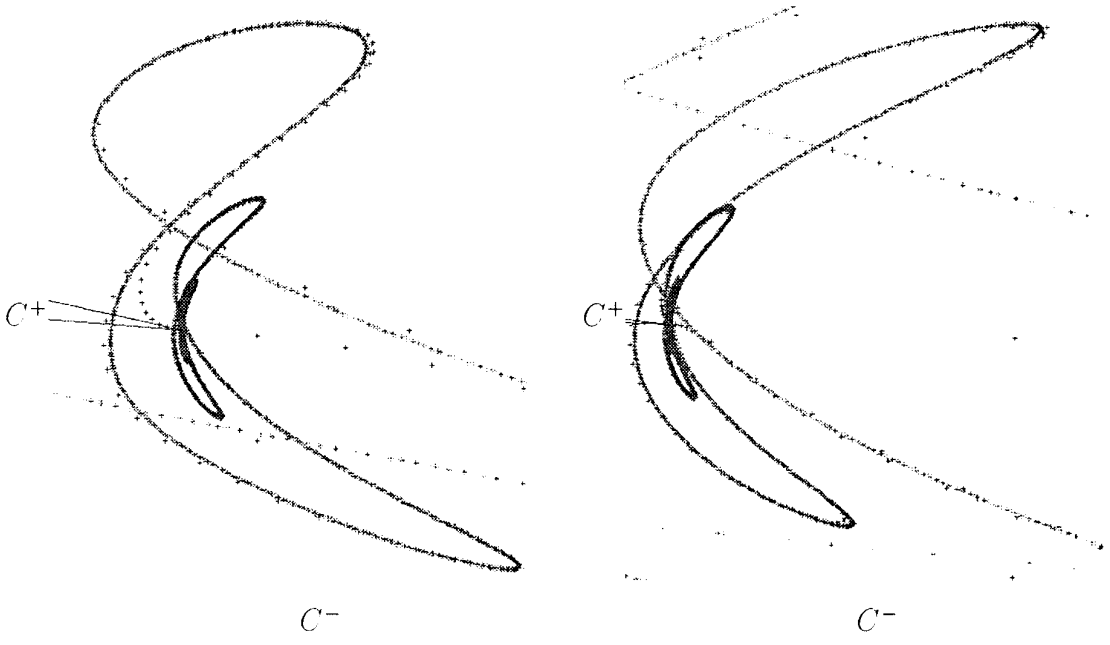

FIG. 15. A zoom of the orbit obtained for the unlimited Lax–Wendroff scheme for the lower lobe (Fig. 14 (left)). These are again for the isothermal Euler equations with stationary shock data $\mathbf{w}_L = (4, -2)^T$, $w_R = (1, -2)^T$, with a superposed convective velocity $u_c = 0.1 = S$. The figure of the left is a blowup of the lower lobe, while the one on the right is a zoom of the first inner lobe, and one can see a self-similar structure. Successive zooms retain this qualitative structure. The view window for the plot on the left is approximately $\Delta C^- = 0.024$, $\Delta C^+ = 1.2$, while that for the plot on the right is approximately $\Delta C^- = 0.005$, $\Delta C^+ = 0.5$.

self-similar structure (Fig. 15), which resembles features observed in dynamical systems. Another observation is that Van Leer's FVS scheme gives a classic spiral at the left-state (Fig. 14). Thus, the phase portraits present a rich variety of striking features that we could not possibly have anticipated.

5. DIAGNOSIS OF THE PROBLEM

What we have observed so far indicates that postshock oscillations are not merely a *slow* or *fast* shock effect. Further, the Osher scheme is as prone to them as the Roe scheme, and the error is not limited to any one acoustic family. We now formulate an explanation of the postshock oscillations, with the isothermal Euler equations as illustration.

5.1. The Cause of the Postshock Oscillations

Consider data that corresponds exactly to a single front-shock for some conservation law. To bring out the difficulty, we will suppose it to be a slowly moving shock, even though that is not essential as we have already seen. We might intuitively suppose that the orbit generated by a slowly moving shock would be a perturbation around the locus of intermediate states representing stationary shocks at different locations relative to the grid. In other words, we might hope, with encouragement from Fig. 10, to develop a quasi-stationary theory of slowly moving shocks. Roe [31] has shown that stationary shocks produced by the Godunov or Roe schemes have just one intermediate state, which lies on H (where the correct H is the 2-shock (1-shock) curve for a corresponding shock through the left (right) state). Because of its relevance we reproduce the proof.

Consider the isothermal Euler equations and assume we have supersonic flow to the left (i.e., the right state is supersonic to the left as shown in Fig. 16). Then $\mathbf{F}_{MR} = \mathbf{F}_R$. For a stationary shock, we require $\mathbf{F}_L = \mathbf{F}_{LM} = \mathbf{F}_{MR} = \mathbf{F}_R$, and $\mathbf{F}_L = \mathbf{F}_R$ is given. However, if there are to be no waves created that go leftward at the L, M interface, then we need $\hat{\alpha}_1 = 0$, where

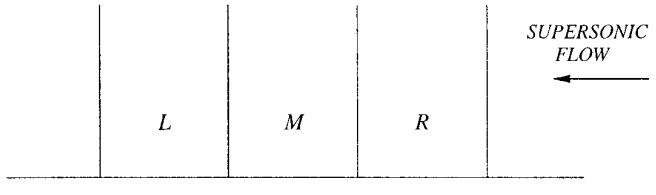

FIG. 16. Schematic of the stationary shock structure for the Roe scheme, illustrated on the isothermal Euler equations. States to the right of R are all equal to R and supersonic to the left, while those to the left of L are similarly equal to L. M is the middle state within which the shock is trapped. Since it is a stationary shock, $\mathbf{F}_L = \mathbf{F}_{LM} = \mathbf{F}_{MR} = \mathbf{F}_R$.

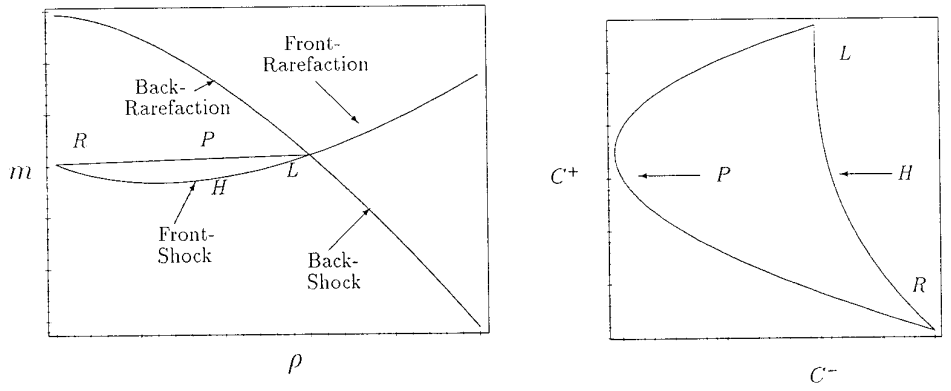

FIG. 17. On the left, we present the shock and rarefaction curves for the isothermal Euler equations in conserved variable space, showing the loci of right states that can be connected to the given left state (L) by a single wave (shock or rarefaction). Further, selecting a 2-shock (front-shock) which is also the relevant Hugoniot H, we show the right state (R) and the projection (P), which is the set of intermediate states that can be formed by a moving discontinuity of arbitrary speed, after exactly one time step. From conservation, these states must lie on the straight line joining the left and right states in conserved variable space. Notice that H is not monotone in this space. The figure on the right is the relevant part of the one on the left, showing the states (L, R), the Hugoniot (H), and the projection (P), but shown in characteristic variable space. Notice that P is not monotone in this space, while H is so.

$$\hat{\alpha}_1 = \frac{1}{2}\left(\Delta\rho - \frac{\hat{\rho}}{a}\Delta u\right), \quad \hat{\rho} = (\rho_L \cdot \rho_R)^{1/2};$$

i.e., we have a vanishing 1-wave. This implies that

$$\Delta u = \frac{a}{\hat{\rho}}\Delta\rho,$$

which can be easily rearranged to give

$$m = \frac{\rho}{\rho_L} m_L + (\rho - \rho_L)\, a \left(\frac{\rho}{\rho_L}\right)^{1/2}.$$

But this is exactly the 2-shock curve [15] connecting L to M, demonstrating that the single intermediate state M lies on the nonphysical branch of the Hugoniot through L, thus generating no leftward propagating waves. This also ensures equality of all fluxes, satisfying stationarity of the shock. It is plausible that when the shock is slowly moving, M will lie slightly off H, giving rise to weak left-moving waves.

Now consider the projection onto the grid of a shock not lying at an interface (Fig. 17 (left)). For different locations of the shock within the cell (Fig. 1 (left)), the locus of the projection P (i.e., the set of intermediate states M that can be formed by a moving discontinuity of arbitrary speed, after exactly one time step) in the space of conserved variables (ρ, ρu) is a straight line joining states L and R (from conservation). If it were possible to create a scheme that could capture a moving shock (of any speed) with a single intermediate state at all times, that state, by conservation, would have to lie on P. Moreover, after the first time step, the solitary intermediate state generated for either the Roe scheme or the Godunov scheme by a moving shock does lie on P (from conservation, and the ability of each of these schemes to recognize isolated shocks). Many of the orbits that we have observed seem to be ''influenced'' by both H and P. Transferring these curves (H and P) to characteristic variables space (C^-, C^+), we find that while the Hugoniot H is monotone, the projection P is not (Fig. 17 (right)).

A critical point to note is that if the intermediate point M is not on H, a nonvanishing left-going wave *will* be generated by the Riemann problem (L, M), since from Fig. 17 (left) we notice that any point lying on P is connected to L by a combination of a back-rarefaction and a front-shock.

The root of the postshock oscillations now lies exposed; most numerical schemes that solve Riemann problems take as input the projections of the solution in each cell (or some higher order interpolation based on the same projections). As we have seen, this leads to a full set of waves of nonvanishing strength (since H and P are distinct, in general), which are continuously generated and contaminate our numerical solution. An alternative explanation is that a shock that did not generate spurious waves would have to stay close to the quasi-steady trajectory H; such a shock could not be conservative.

According to this explanation, if we could devise a nonlinear case where P and H are coincident, we would expect no oscillations, since after one time-step M would be on P. However, this also being H, we can still connect L to M by a single shock, leading to no backward waves being generated, and this process would be expected to continue for all time. Such a situation arises in a class of problems where the nonlinearity is purely quadratic. These were

studied in detail in [32], where the specific cases were classified.

5.2. A Model Problem with Quadratic Nonlinearities

This system may again be written in the form of Eq. (2.1), with

$$\mathbf{w} = (u, v)^{\mathrm{T}}, \quad \mathbf{f} = (au^2 + v^2, 2uv)^{\mathrm{T}}, \quad a = \text{const}, \tag{5.1}$$

and with wavespeeds

$$\lambda_{1,2} = u(1 + a) \mp [u^2(a - 1)^2 + 4v^2]^{1/2}, \quad \lambda_1 < \lambda_2. \tag{5.2}$$

The characteristic equations are

$$2v\, du + (\lambda_{1,2} - 2au)\, dv = 0, \quad \text{along } \frac{dx}{dt} = \lambda_{1,2}$$

However, characteristic variables are not readily available in closed form.

A simple feature of this system is that since the nonlinearity is purely quadratic, the Roe matrix $\hat{\mathbf{A}}$ is simply $\mathbf{A}$ evaluated at the average state, i.e.,

$$\hat{\mathbf{A}} = \overline{\mathbf{A}} = \mathbf{A}\,(\overline{\mathbf{w}}), \quad \text{where } \overline{\mathbf{w}} = \tfrac{1}{2}(\mathbf{w}_{\mathrm{L}} + \mathbf{w}_{\mathrm{R}}).$$

The Hugoniot is

$$(a - 1)\,\overline{u}\,[u]\,[v] + \overline{v}\,[v]^2 - \overline{v}\,[u]^2, \quad u_{\mathrm{R}} < u_{\mathrm{L}}, \tag{5.3}$$

where $[z] = z_{\mathrm{R}} - z_{\mathrm{L}}$ denotes the jump in quantity z. This equation can be easily solved for $[u]$ and substituted into the expression for the shock speed $S = [\mathbf{f}]/[\mathbf{w}]$, resulting in a shock speed that is merely the characteristic speed $\lambda_{1,2}$ evaluated at the average state $\overline{\mathbf{w}}$.

A special case for this model arises when we choose initial data satisfying

$$v = \alpha u, \quad \alpha = (2 - a)^{1/2}, \quad a < 2.$$

This straight line identically satisfies Eq. (5.3), and if $u_{\mathrm{R}} < u_{\mathrm{L}}$ is chosen, then we get entropy-satisfying shocks. Since u, v are conserved variables, this line is also the projection. Thus, for this choice of initial data, the Hugoniot H and projection P coincide. Numerical experiments verify that the solution is indeed oscillation-free, although data not lying on this line do generate oscillations.

5.3. A Conjecture

The result that the locus of intermediate state for a stationary shock coincides with the nonphysical branch of the Hugoniot through the postshock state can be shown to hold for either the Godunov or Roe fluxes, for any set of equations in which the nonlinear waves are convex. Our results above lead us to make the following conjecture:

Slowly moving shockwaves will generate spurious oscillations in a code employing either the Godunov or Roe fluxes whenever the Hugoniot curves are not straight lines in the phase space of conserved variables. For other fluxes giving rise to one-point stationary shocks, the locus that must be a straight line is the locus traced by that intermediate point.

For schemes creating two- or more-point shocks, it is possible to satisfy conservation without having the intermediate points follow the straight path P. For example, if two intermediate states are involved, it is necessary and sufficient that their centroid remains on P. To date, however, we have not seen how to use this additional freedom in any advantageous way.

6. SOME POSSIBLE CURES

We incline to the belief that postshock oscillations are an inevitable feature of shocks captured by currently standard methods, except for certain special equation sets. However, we list below some unorthodox strategies that could be worth investigating in more depth than we had time to achieve.

6.1. Adaptive Grids with Dissipative Schemes

An obvious remedy, which is viable and available, is to use a sufficiently dissipative scheme in the entire domain and to regain the resolution of the flow features by grid adaptation [3, 28]. But for unsteady problems, additional adaptation results in time-step penalties, which may be quite severe if we want to maintain time-accuracy. This expense can be substantially reduced if we take (many) smaller time-steps in fine-mesh regions, while taking larger steps in other regions (see, for example, [28]), since the fine-mesh regions are typically a small fraction of the computational domain. Since the minimum-dispersion scheme used by itself as a first-order scheme yielded rather small oscillations in Section 2.3, we experimented with a second-order limiter scheme in which the minimum-dispersion scheme was used as the low-order component. We again found oscillations but did not explore the full range of combinations for high- and low-order schemes and limiter strategies. We note that *some* form of controlled shock spreading has been the cure recommended by several investigators [38, 5, 17].

6.2. Physical Viscosities

We conducted some experiments on a kinetic-upwind scheme in which the numerical flux is derived by considering the distribution of random velocities in each cell. A particular version is based on assuming that the velocities

are relaxing toward equilibrium according to the BGK approximation [39, 27]. Although originally conceived as a strategy for the Euler equations, it turns out that it simulates the Navier–Stokes equations at some local Reynolds number. It might be found appealing that the artificial viscosity should actually be a natural one, although to some extent, this is a return to the concepts of von Neumann and Richtmyer [23]. However, the results were, once again, oscillatory. We are not sure whether a sufficiently smart adaptation of the viscosity coefficients would help. Note that the oscillatory behavior observed for this scheme demonstrates that it is not just schemes based on Riemann solvers that are plagued.

6.3. Shock Recovery

We also implemented a scheme that uses a form of subcell resolution to enable *shock recovery*. Estimating the shock location from the position of inflection points, the correct fluxes could be applied at the interfaces ($\mathbf{F}_L$ on LM and $\mathbf{F}_R$ on MR) while the shock was in cell M. In addition, if the shock were to move out of M in the current time-step, the time-step was split into two parts. Such a scheme forces the intermediate states to follow P, as desired, and retains a single intermediate point. Some results using such a "fix" were given in [1]. A multidimensional version of this strategy would, however, be very complicated.

7. CONCLUDING REMARKS

It is quite possible that there is, in general, no completely satisfactory solution to this problem. The decision to capture shockwaves (and contacts) rather than to fit them, surely carries *some* unavoidable penalties, at least if we also attempt to resolve them as sharply as possible. Two decades of practical success have shown that in many contexts, the penalties are not too severe, but as Quirk [28] has pointed out, increasingly ambitious applications tend to probe the weaknesses of even widely employed algorithms.

The phenomenon under study is likely to be significant for computational aeroacoustics, where the acoustic signals may be several orders of magnitude less energetic than the mean flow and could well become confused with oscillations generated by almost stationary shockwaves. Simply designing the scheme to be "monotone" or "TVD" does not solve the problem because we have shown that there are no entirely satisfactory nonlinear definitions of these terms, even in one dimension.

In principle, a solution that is simple to implement is to employ a sufficiently dissipative (and largely oscillation-free) scheme and to regain the resolution by means of an adaptive grid. This would be an expensive option if implemented naively. One would like to think that the decades of investment in high-resolution schemes could make a more rational contribution.

A return to the mathematically impeccable strategy of shock-fitting should of course eliminate the difficulty, but the numerical hardships are formidable if there are multiple shocks with many intersections. Interesting compromises involve shock recovery [22], floating shock-fitting [21, 10], and grid adjustment [16, 26, 37].

ACKNOWLEDGMENT

We thank Dr. Kun Xu for providing his flow solver based on the BGK approximation and for his help in running some benchmark cases for the Euler equations on that solver.

REFERENCES

1. M. Arora and P. L. Roe, "On Oscillations due to Shock Capturing in Unsteady Flows," in *Proceedings,* 14*th International Conference on Numerical Methods in Fluid Dynamics* (Springer-Verlag, New York, 1994).
2. M. Arora and P. L. Roe, *J. Comput. Phys.* **128** (1995).
3. M. J. Berger and P. Colella, *J. Comput. Phys.* **82,** 64 (1989).
4. J. P. Boris and D. L. Book, *J. Comput. Phys.* **1,** 38 (1973).
5. P. Colella, *SIAM J. Sci. Statist. Comput.* **6,** 104 (1985).
6. B. Engquist and Q. Huyuh, "Iterative Gradient-Newton Type Schemes for Steady Shock Computations," in *Proceedings, 5th US-Mexico Workshop—Advances in Numerical ODEs and Optimization, SIAM, 1989.*
7. S. K. Godunov, *Mat. Sb.* **47,** 271 (1959).
8. J. J. Gottlieb and C. P. T. Groth, *J. Comput. Phys.* **78,** 437 (1988).
9. A. Harten, *J. Comput. Phys.* **49,** 357 (1983).
10. P. M. Hartwich, *AIAA J.* **32,** 1791 (1994).
11. T. Hou and P. D. Lax, *Commun. Pure. Appl. Math.* **44,** 1 (1991).
12. A. Jameson, *Int. J. Comput. Fluid Dyn.* **4,** (1995).
13. G. Jennings, *Commun. Pure Appl. Math.* **27,** 25 (1974).
14. P. D. Lax and B. Wendroff, *Commun. Pure Appl. Math.* **13,** 217 (1960).
15. R. J. LeVeque, *Numerical Methods for Conservation Laws* (Birkhauser, Basel, 1990).
16. R. J. LeVeque and K. M. Shyue, in preparation.
17. H.-C. Lin, *J. Comput. Phys.* **117,** 20 (1995).
18. M.-S. Liou, "Progress towards an Improved CFD Method: AUSM+," in *AIAA 12th Computational Fluid Dynamics Conference, AIAA, 1995,* p. 606.
19. A. J. Majda and J. Ralston, *Commun. Pure Appl. Math.* **32,** (1979), p. 445.
20. D. Michaelson, *Adv. in Appl. Math.* **5,** 433 (1984).
21. G. Moretti, *Comput. & Fluids* **15,** 59 (1987).
22. K. W. Morton and M. A. Rudgyard, "Finite Volume Methods with Explicit Shock Representation," in *Computational Aeronautical Fluid Dynamics,* edited by L. Fezoui, J. Periaux, and J. C. R. Hunt (Clarendon, Oxford, 1989), p. 103.
23. J. V. Neumann and R. D. Richtmyer, *J. Appl. Phys.* **21,** 232 (1950).
24. S. Osher, *SIAM J. Numer. Anal.* **21,** 217 (1984).
25. S. Osher and F. Solomon, *Math. Comput.* **38,** 339 (1982).
26. M. Paraschiviou, J. Y. Trepanier, M. Reggio, and R. Camarero, *AIAA* paper, 1994.
27. K. H. Prendergast and K. Xu, *Comput. Phys.* **109,** 53 (1993).

28. J. J. Quirk, *Int. J. Numer. Methods Fluids* **18,** 555 (1994).
29. T. W. Roberts, *J. Comput. Phys.* **90,** 141 (1990).
30. P. L. Roe, *J. Comput. Phys.* **43** (1981).
31. P. L. Roe, "Fluctuations and Signals, a Framework for Numerical Evolution Problems," in *Numerical Methods in Fluid Dynamics*, edited by K. W. Morton and M. J. Baines (Academic Press, New York, 1982, p. 219.
32. D. G. Schaeffer and M. Shearer, *Commun. Pure Appl. Math.* **40,** 141 (1987).
33. J. Smoller, *Shock Waves and Reaction-Diffusion Equations* (Springer-Verlag, New York, 1983).
34. Y. S. Smyrlis, *Commun. Pure Appl. Math.* **42,** 509 (1990).
35. P. K. Sweby, *SIAM J. Numer. Anal.* **21,** 995 (1984).
36. B. van Leer, ICASE Report 82-30, 1982 (unpublished).
37. J. van Rosendale, ICASE Report 94-89, 1994 (unpublished).
38. P. R. Woodward and P. Colella, *J. Comput. Phys.* **54,** 115 (1984).
39. K. Xu, private communication.
40. S.-H. Yu, Ph.D. thesis, Stamford University, 1994.